Vibronic fine structure in the nitrogen 1*s* photoelectron spectra from Franck-Condon simulations. III. Rules for amine and imine N atoms in small *N*-heterocycles

Minrui Wei,[1] Junxiang Zuo,[1] Guangjun Tian,[2,*] and Weijie Hua[1,†]

[1]*MIIT Key Laboratory of Semiconductor Microstructure and Quantum Sensing, Department of Applied Physics, School of Physics, Nanjing University of Science and Technology, 210094 Nanjing, China*

[2]*Key Laboratory for Microstructural Material Physics of Hebei Province, School of Science, Yanshan University, 066004 Qinhuangdao, China*

(Received 8 November 2023; accepted 31 January 2024; published 28 February 2024)

Vibronic coupling plays a crucial role in x-ray photoelectron spectra (XPS) of molecules. In a series of three papers, we present a comprehensive exploration of the *N*-heterocycles family, known for their diverse structures, to summarize the general rules of vibronic coupling in high-resolution vibrationally resolved XPS spectra at the N 1*s* edge. Building upon our previous studies on six-membered monocyclic azines [Phys. Rev. A **106**, 022811 (2022)] and fused bicyclic compounds indoles with five and six members [Phys. Rev. A **108**, 022816 (2023)], in this study, we focus on investigating a series of 12 five-membered *N*-heterocycles using Franck-Condon simulations, incorporating Duschinsky rotation effects and density functional theory. Our calculations reveal distinct spectral characteristics of amine and imine within these 12 systems in binding energies, spectral characteristics, structural changes, vibrational coupling strengths, and effects of hydrogenation. Furthermore, we expand our analysis to encompass all 35 *N*-heterocycles discussed in the three papers and consolidate these findings into the general rules. We find that 1*s* ionization in amine nitrogen induces more substantial geometrical changes, resulting in larger vibronic coupling strength compared to imine nitrogens. The spectra of imine nitrogens exhibit two distinct characteristic peaks originating from the 0-0 and 0-1 transitions, whereas the spectra of amine nitrogens are characterized by a broad peak with numerous weak fingerprints due to significant mixing of various 0-*n* transitions. We observe that amine (imine) nitrogens generally cause a negative (positive) change in zero-point vibrational energy. This study provides valuable insights into vibronic coupling in *N*-heterocycles, shedding light on the distinguishing features and behavior of amine and imine nitrogens in vibrationally resolved XPS spectra.

DOI: 10.1103/PhysRevA.109.022820

I. INTRODUCTION

X-ray photoelectron spectroscopy (XPS) is one of the most successful spectroscopic techniques and is widely used in molecules and materials. Existing experimental databases for XPS [1–8] collect important reference data for a large number of molecules and materials, which facilitate spectral interpretation and help to interpret the physical and chemical insights behind the data [9–11]. However, most libraries report only binding energy (BE) data (sometimes with inconsistency) and important spectral profile information is missing. A high-resolution theoretical library is urgently needed to reveal the physical nature and provide a better reference for the structural characterization.

Vibronic coupling plays an important role in XPS which defines its high-resolution fine structures. To understand the physical nature of vibronic coupling in molecular XPS spectra, we focused on the nitrogen-heterocycle compounds and performed accurate theoretical calculations for a number of molecules. These compounds, which only contain three elements, C, N, and H, are important building blocks in the fields of photochemistry, biology, materials science, and pharmacy, and exhibit rich structural flexibility to study structure-spectroscopy relationships. The search for the rules of vibronic coupling is a necessary preliminary study for the automatic construction of a theoretical library with a large number of molecules. This is because the computation for excited states with a core hole is challenging and sometimes convergence problems occur during the self-consistent field or geometric optimization steps.

We would like to follow up on the early pioneering work of Siegbahn [9,12–17], who investigated families of systems by high-resolution experiments and calculations, and simulate the accurate vibrationally resolved XPS of molecules with similar structures on the same basis. In previous papers of this series, we have systematically studied azines [18] (paper I) and indoles [19] (paper II). These are monocyclic compounds with six-membered rings and bicyclic compounds consisting of fused five- and six-membered rings, respectively. Good agreement was obtained with the experiments and some general structure-spectroscopy rules were established. Therefore, it is natural and necessary to investigate the performance of pure five-membered ring compounds in this work (paper III).

*tian@ysu.edu.cn
†wjhua@njust.edu.cn

A total of 12 monocyclic compounds with five-membered rings were selected in this study. These include two pyrrole and three pyrroline isomers, pyrazoline, two diazoles (imidazole and pyrazole), three triazoles (1,3,4-triazole, 1,2,5-triazole, and 1,2,4-triazole), and one anion *cyclo*-N_5^-. Pyrrole and imidazole are essential building block molecules in biological systems and are found in compounds, such as amino acids (e.g., tryptophan and histidine) and porphyrins [20–22]. Pyrroline, on the other hand, is commonly found in natural products, drug molecules, and synthetic intermediates. It has various applications in medicine [23–26] and pesticides [26,27]. Although pyrazole is rare in nature, its derivatives exhibit diverse pharmacological activities [28]. Triazoles have significant potential for applications in nitrogen-rich high-energy density materials (HEDMs) due to their high thermal stability and positive enthalpy of formation [29,30]. The cyclopentazole anion *cyclo*-N_5^- represents an important structural motif and has attracted significant research interest in recent years [31–33].

To our knowledge, XPS experiments [2] on these compounds are relatively outdated and have low resolution. Core binding energies were reported for part of systems like pyrrole [2,34–36] and imidazole [37]. While gas-phase N 1*s* XPS spectra have been measured for pyrrole, the limited precision hampers further vibronic analysis [2]. Solid-state BE measurements are also accessible (e.g., pyrazole [38]), but the crystal surroundings cause the BEs (and spectral profiles) to differ from those in the gas phase. In light of this, our study aims to provide accurate and vibrationally resolved N 1*s* XPS spectra for 12 commonly encountered five-membered heterocyclic complexes. Moreover, we endeavor to establish general rules for small *N*-heterocycles based on comprehensive data acquired throughout the three papers in this series. Our analyses will encompass chemical shifts, fine structures, vibronic transitions, and active vibrational modes, and will particularly focus on distinguishing features between amine (-N <) and imine (=N-) nitrogens.

In small molecules, amine and imine nitrogens exhibit characteristic 1*s* binding energies [39]. The two bonding types are essential components in a wide variety of large systems, including DNA [40], enzymes [41], coordination complexes (as ligands) [42], and so on. Amine and imine nitrogens have become valuable building blocks for synthetic chemists, with wide applications in supramolecular and dynamic covalent chemistry [43,44], and the synthesis of covalent organic frameworks (COFs) [45,46]. It would be meaningful to investigate the intrinsic properties of amine and imine nitrogens, although in complex material environment may also enforce interactions. 1*s* electrons are deeply bound in atoms; in this work, we wish to go beyond the core binding energies and study their vibronic properties regarding 1*s* core ionizations.

The structure of this work is organized as follows. Section II briefly outlines the computational details employed in this study. Subsequently, in Sec. III, we present the results obtained for the 12 five-membered molecules. In Sec. IV, we summarize the general vibronic rules derived from the complete data set encompassing 35 molecules across all three papers. Finally, we provide concluding remarks and an outlook for future research.

II. COMPUTATIONAL DETAILS

The computational methods were described in detail previously [18,19], so that only brief expositions are given here. All electronic structure calculations were performed using the GAMESS-US package [47,48] at the density functional theory (DFT) level with the B3LYP functional [49–51]. The vibronic fine structure was calculated using a modified DYNAVIB package [52,53]. Within the harmonic oscillator approximation, the Duschinsky rotation (DR) effect [54] was included to calculate the Franck-Condon (FC) factors. The normal modes of the ground ($\mathbf{q}'$) and core-ionized ($\mathbf{q}$) electronic states, described by column vectors, are linearly related by the Duschinsky transformation, $\mathbf{q}' = \mathbf{J}\mathbf{q} + \mathbf{k}$. Here $\mathbf{J}$ and $\mathbf{k}$ refer to the Duschinsky rotation matrix and the displacement vector, respectively. The FC amplitude $\langle 0|0\rangle$ was computed based on vibrational frequencies and displacements, and then amplitudes $\langle 0|n\rangle$ in a recursive manner starting from $\langle 0|0\rangle$ [55–57]. The FC factor is computed as the square of the FC amplitude. No temperature effect was considered (i.e., $T = 0$ K).

From the electronic structure calculations, we obtained the vertical (I^{vert}) and adiabatic (I^{ad}) ionic potentials (IPs) and the difference of zero-point vibrational energies (ZPE) between the final full core hole (FCH) state and the initial ground state (GS) ($\Delta\varepsilon_0$). We followed our previous studies [18] to use DR to label the 0-0 vibrational transition energy as E_{00}^{DR} (to distinguish with the linear coupling method [58,59] within the framework of Frank-Condon simulations) [18,19]:

$$I^{\text{vert}} = E_{\text{FCH}}|_{\textbf{min GS}} - E_{\text{GS}}|_{\textbf{min GS}} + \delta_{\text{rel}}, \tag{1}$$

$$I^{\text{ad}} = E_{\text{FCH}}|_{\textbf{min FCH}} - E_{\text{GS}}|_{\textbf{min GS}} + \delta_{\text{rel}}, \tag{2}$$

$$\Delta\varepsilon_0 = \varepsilon_0^{\text{FCH}} - \varepsilon_0^{\text{GS}}, \tag{3}$$

$$E_{00}^{\text{DR}} = I^{\text{ad}} + \Delta\varepsilon_0. \tag{4}$$

Here E_{GS} and E_{FCH} stand for the total energies of the GS and FCH states, respectively. **min GS** and **min FCH** denote optimized structures of the two states. To account for the scalar relativistic effect of the N 1*s* core hole, the calculated IPs were calibrated by adding a uniform shift of $\delta_{\text{rel}} = 0.3$ eV [60].

Stick spectra were convoluted with a Lorentzian line shape function. Half width at half width at half maximum (HWHM) of $\gamma = 0.05$ eV was used for most systems [18,19]. To better visualize the profile details, slightly smaller $\gamma = 0.04$ eV (for 2-pyrroline) and $\gamma = 0.03$ eV (for pyrrole and cyclo-N_5^-) were used. It is necessary to note that, for simplicity, here γ is to phenomenologically take into account the influence of all factors (lifetime, instrument resolution, nuclear motion, environmental effect, etc.) on the experimental linewidth, which are smaller than the experimental N 1*s* core-hole HWHM lifetime of 0.065 eV [61]. For more advanced broadening, one can turn to the Voigt convolution with separated influences of the lifetime (Lorentzian) and other factors (Gaussian) [62]. The convergence threshold for the FC factors was set at 0.99 throughout this work. For molecules with multiple nitrogens, the sum of individual atom-specific spectra leads to the total spectrum. All raw numerical data for the theoretical spectra and Cartesian coordinates of the optimized geometries are available online [63].

TABLE I. Vertical and adiabatic ionization potentials ($I^{\rm vert}$ and $I^{\rm ad}$), their difference (ΔI), the 0-0 transition energy ($E_{\rm DR}^{00}$), and the ZPE difference ($\Delta\varepsilon_0$) [see Eqs. (2) and (3)] of all systems simulated with B3LYP. All energies are in eV. N* denotes the core-ionized N atom; amine (bold) and imine (normal) N atoms are indicated by different fonts. Relative deviations to experiments are given in parentheses.

Molecule	N*	Expt.	$I^{\rm vert}$	$I^{\rm ad}$	ΔI	$E_{00}^{\rm DR}$	$\Delta\varepsilon_0$
2H-pyrrole	N		404.20	404.06	0.14	404.10	0.04
1-pyrroline	N		404.37	404.21	0.16	404.23	0.02
3-pyrroline	**N**		404.50	404.21	0.29	404.23	0.02
2-pyrroline	**N**		404.84	404.57	0.27	404.57	0.00
1H-pyrrole	**N**	406.15[a]/406.10[b]/ 406.00[c]/406.18[d]	406.03 (−0.12/0.07/ +0.03/−0.15)	405.76 (−0.39/ − 0.34 −0.24/−0.42)	0.27	405.73	−0.03
imidazole	**N1**	405.60[e]	406.59 (+0.99)	406.23 (+0.63)	0.36	406.16	−0.07
	N2	403.90[e]	404.25 (+0.35)	404.06 (+0.16)	0.19	404.10	0.04
pyrazole	**N1**		406.83	406.45	0.38	406.38	−0.07
	N2		405.10	404.94	0.16	404.96	0.02
2-pyrazoline	**N1**		405.41	405.06	0.35	405.03	−0.03
	N2		405.32	405.16	0.16	405.16	0.00
1, 3, 4-triazole	**N1**		407.23	406.86	0.37	406.78	−0.08
	N2		405.21	405.04	0.17	405.06	0.02
1, 2, 5-triazole	**N1**		407.87	407.39	0.48	407.30	−0.09
	N2		405.98	405.80	0.18	405.79	−0.01
1, 2, 4-triazole	**N1**		407.44	407.02	0.42	406.93	−0.09
	N2		405.71	405.53	0.18	405.53	0.00
	N3		404.91	404.69	0.22	404.71	0.02
cyclo-N_5^-	N		400.58	400.28	0.30	399.98	−0.03

[a]Jolly *et al.* [2].
[b]Gelius *et al.* [34].
[c]Pan *et al.* [35].
[d]Cavell *et al.* [36].
[e]Nolting *et al.* [37].

III. RESULTS FOR FIVE-MEMBERED *N*-HETEROCYCLES

A. Statistics on IPs

Table I presents the vertical (adiabatic) N 1*s* IPs calculated by B3LYP for all systems and the visualization is also provided in Fig. S1. The only anion *cyclo*-N_5^- exhibits the lowest vertical (400.6 eV) and adiabatic (400.3 eV) IPs, which differs significantly from the remaining molecules. For these molecules, there are a total of 20 N centers, comprising 9 amine and 11 imine nitrogen atoms. The vertical (adiabatic) IPs range from 404.2 to 407.9 eV (404.1 to 407.4 eV) spanning a range of 3.7 eV (3.1 eV). Amine and imine nitrogens can be readily distinguished based on their IPs: amine N atoms generally show larger vertical (adiabatic) IPs of 404.5–407.9 eV (404.2–407.0 eV), whereas imine N atoms have IPs ranging over 404.2–406.0 eV (404.1–405.8 eV). It should be noted that there is some overlap between the two regions.

The core ionization-induced structural relaxation effect in the excited-state potential energy surface (PES) can be estimated by calculating the difference between vertical and adiabatic IPs, defined as

$$\Delta I \equiv I^{\rm vert} - I^{\rm ad} = E_{\rm FCH}|_{\rm min\,GS} - E_{\rm FCH}|_{\rm min\,FCH}. \quad (5)$$

This difference of ionization potential, ΔI, is always nonnegative. Our calculations revealed that amine nitrogen atoms (0.3–0.5 eV) exhibit larger ΔI values compared to imine nitrogen atoms (0.1–0.2 eV). This indicates that amine nitrogens undergo larger changes in geometrical structure compared to imine nitrogens.

Our theoretical results agree well with the experiments [2,34–37]: the deviations ranged from −0.2 to 1.0 eV for the vertical IPs and from −0.4 to 0.6 eV for the adiabatic IPs. It is necessary to mention that experimental IP value is usually read from the center of the broadened spectral profile. Calculations based on vertical and adiabatic IPs provide complementary information for comparison. Here, these discrepancies are consistent with the typical accuracy range of 0.5–1.0 eV observed in the ΔKohn-Sham method for predicting 1*s* binding energies of light elements [39,64–67].

B. Changes in structure

Table II summarizes the local structural parameters near the ionized nitrogen (N*) for all molecules at the optimized FCH state and the changes compared to the corresponding optimized ground state. We note that, at each N site, the two N–*X* (X = C, N) distances (in the ground state) exhibit a more pronounced accordance with the Kekulé structures, demonstrating a distinct pattern of one long and one short distance. Let us use N_a and N_i to denote an amine and imine nitrogen, respectively. The N*-*X* bond lengths exhibit distinct differences for the two types: N_a^*-*X* is consistently elongated compared to the ground state, whereas N_i^*-*X* can either be elongated or shortened. The variation of N*-*X* of amine N atoms (0.00–0.17 Å) is larger than that of imine N atoms (0.00–0.06 Å). All N_a^*-H bond lengths are found to be 0.97–0.98 Å, which are reduced by 0.02–0.04 Å compared to those in the GS geometries. Meanwhile, we observed a consistent

TABLE II. Structures in the final-state geometry (**min FCH**) of each molecule, changes (included in parentheses) to the ground-state geometry (**min GS**), and RMSD values (in Å) between them (superimposed subject to the smallest RMSD). Only the bond lengths (in Å) and angles (in deg) surrounding each ionized nitrogen atom (N*) are listed. Amine N (N_a^*) (boldface); imine N (N_i^*) (lightface).

Molecules	N*	N_a^*-C	N_a^*-H	N_i^*-C	∠C-N_a^*-C	∠C-N_i^*-C	RMSD
2H-pyrrole	N			1.44(−0.02); 1.29(+0.00)		109.2(+3.2)	0.03
1-pyrroline	N			1.50(+0.03); 1.25(−0.01)		112.3(+3.5)	0.04
3-pyrroline	**N**	1.50(+0.03); 1.50(+0.03)	0.97(−0.04)		112.9(+3.5)		0.10
2-pyrroline	**N**	1.46(+0.06); 1.52(+0.04)	0.97(−0.04)		109.0(+3.0)		0.15
1H-pyrrole	**N**	1.44(+0.07); 1.44(+0.07)	0.98(−0.02)		108.7(−1.2)		0.03
imidazole	**N1**	1.49(+0.13); 1.43(+0.05)	0.98(−0.02)		104.7(−2.6)		0.05
	N2			1.37(+0.00); 1.31(+0.00)		109.1(+3.6)	0.04
pyrazole	**N1**	1.51(+0.17);[a] 1.40(+0.04)	0.98(−0.03)		110.5(−2.7)[c]		0.05
	N2			1.34(+0.00);[b]1.34(+0.01)		107.0(+2.8)[e]	0.04
2-pyrazoline	**N1**	1.55(+0.15);[a] 1.48(+0.00)	0.98(−0.02)		110.8(+2.3)[c]		0.09
	N2			1.45(+0.06);[b]1.26(−0.02)		111.2(+2.4)[e]	0.04
1, 3, 4-triazole	**N1**	1.46(+0.09); 1.46(+0.09)	0.98(−0.02)		102.1(−2.5)		0.04
	N2			1.41(+0.03);[b]1.29(−0.02)		110.3(+2.9)[e]	0.03
1, 2, 5-triazole	**N1**	1.45(+0.12);[a]1.45(+0.12)[a]	0.98(−0.02)		113.7(−2.9)[d]		0.07
	N2			1.33(−0.00); 1.34(+0.00)[b]		105.2(+2.5)[e]	0.04
1, 2, 4-triazole	**N1**	1.50(+0.14);[a]1.42(+0.07)	0.98(−0.02)		107.2(−3.1)[c]		0.05
	N2			1.35(−0.01);[b]1.34(+0.02)		104.4(+2.5)[e]	0.04
	N3			1.37(+0.00); 1.31(+0.00)		106.2(+3.4)	0.04

[a] N_a^*-N.
[b] N_i^*-N.
[c] ∠C-N_a^*-N.
[d] ∠N-N_a^*-N.
[e] ∠C-N_i^*-N.

increase in the bond angle ∠C-N_i^*-X upon ionization of the imine N atoms. The increment ranges over 3.2–3.6° when X represents carbon and 2.4–2.9° when X represents nitrogen. However, for amine N atoms, the bond angle ∠X-N_a^*-X decreases for almost all molecules, except for the nonplanar molecules 2-pyrroline, 3-pyrroline, and N1 in 2-pyrazoline.

To reflect the global structural change, the root-mean-squared deviation (RMSD) values between the two structures were calculated and listed in Table II. Generally, amine nitrogens (0.03–0.15 Å) give larger RMSD values than imine nitrogens (0.03–0.04 Å).

C. Huang-Rhys factors (S_i) and the vibrational reorganization energies (E_r)

Table III presents the computed vibrational frequencies and Huang-Rhys factors (HRFs) for all molecules in their N 1s ionized states. The HRF is defined as follows:

$$S_i = \frac{1}{2\hbar}\omega_i k_i^2. \tag{6}$$

Here, k_i denotes the ith elements of the displacement column vector **k** and ω_i represents the vibrational frequency of mode i in excited state. The square root of the HRF is commonly referred to as the electron-phonon coupling strength (λ_i), that is,

$$\lambda_i = \sqrt{S_i}. \tag{7}$$

In our analysis, we employed a threshold of $S_i \geqslant 0.3$ for all N* atoms (in practice, we used S_i to filter). Amine nitrogen ionizations (2–5 modes) generally correspond to more active vibrational modes than imine nitrogens (1–2 modes). Notably, we observed that only weak electron-phonon coupling ($S_i < 1.0$) was evident across all modes for all imine nitrogens. In contrast, amine nitrogens exhibited modes with intermediate ($S_i \approx 1.0$) or strong ($1.0 \leqslant S_i \leqslant 2.2$) electron-phonon coupling strengths.

It is found that, for imine nitrogen ionizations, at least one ring-deformation mode is Franck-Condon active. This does not hold true for amine nitrogen ionizations. In the latter case, N-X stretching modes (where X is a C or N atom) are commonly recognized as active, typically exhibiting strong electron-phonon coupling values. Furthermore, active modes associated with the N-H bonds, such as N-H wagging (3-pyrroline), N-H stretching (3-pyrroline and 1,2,5-triazole), and N-H deformation (3-pyrroline, 1-pyrrole, and imidazole) are also found for amine N ionizations in some molecules. We also calculated the total vibrational reorganization energy as given by,

$$E_r = \sum_i S_i \hbar\omega_i, \tag{8}$$

for each molecule, which is closely associated with structural changes. Our calculations revealed that amine nitrogens (0.51–0.63 eV) exhibit significantly higher reorganization energy compared to imine nitrogens (0.10–0.34 eV). This indicates that ionization in amine nitrogen atoms induces more pronounced structural deformation than in imine nitrogen atoms [68]. Consequently, it is reasonable to observe

TABLE III. Analysis of selected vibrational modes with large (with a threshold $S_i \geqslant 0.3$) Huang-Rhys factors for the 11 five-membered molecules. Vibrational frequencies ω_i, electron-phonon coupling strength (λ_i), and the total vibrational reorganization energy (E_r) of the excited (FCH) state are given. Amine (bold) and imine (lightface) N atoms are in different fonts.

Molecule	N*	*i*	Approximate assignment	ω_i (cm^{-1})	S_i	λ_i	E_r (eV)
2H-pyrrole	N	4	Ring deformation	849.1	0.70	0.84	0.14
1-pyrroline	N	5	Ring deformation	804.5	0.41	0.64	0.15
3-pyrroline	**N**	3	N-H wagging	406.5	1.39	1.18	0.59
		19	N-H deformation	1401.8	0.85	0.92	
		30	N-H stretch	3855.0	0.50	0.71	
2-pyrroline	**N**	1	Ring torsion	80.6	0.65	0.81	0.32
		6	Ring deformation	759.2	0.33	0.57	
		20	C-H and N-H deformation	1425.7	0.36	0.60	
1H-pyrrole	**N**	12	C-H deformation	1036.9	0.40	0.63	0.34
		18	C-C and C-N stretch	1558.7	1.03	1.01	
imidazole	**N1**	9	C-H deformation	936.1	0.36	0.60	0.58
		10	N-H deformation	945.8	0.31	0.56	
		12	C-C and C-N stretch	1155.4	0.58	0.76	
		16	C-C and C-N stretch	1592.1	1.73	1.32	
	N2	7	Ring deformation	935.7	0.72	0.85	0.18
pyrazole	**N1**	8	Ring deformation	917.6	0.59	0.77	0.61
		9	N-N stretch	969.9	1.32	1.15	
		12	N-N and C-N stretch	1144.4	0.96	0.98	
		13	C-H deformation	1226.3	0.36	0.60	
		14	C-C and C-N stretch	1280.8	0.59	0.77	
	N2	8	Ring deformation	976.6	0.52	0.72	0.16
2-pyrazoline	**N1**	1	Ring torsion	144.0	0.37	0.61	0.51
		6	Ring deformation	800.7	0.70	0.84	
		10	N-N and C-N stretch	932.2	1.04	1.02	
		17	C-H deformation	1339.2	0.50	0.71	
	N2	4	N-H wagging	662.1	0.33	0.57	0.16
		6	Ring deformation	852.6	0.46	0.68	
1,3,4-triazole	**N1**	10	C-H deformation	945.9	0.82	0.91	0.52
		15	C-C and C-N stretch	1625.7	1.76	1.33	
	N2	6	Ring deformation	954.1	0.56	0.75	0.17
		9	N-H deformation	1082.2	0.30	0.55	
1,2,5-triazole	**N1**	7	Ring deformation	935.2	1.95	1.40	0.63
		8	C-H deformation	948.1	0.45	0.67	
		10	N-H stretch	1024.0	1.90	1.38	
		12	C-N stretch	1273.1	0.46	0.68	
	N2	7	Ring deformation	989.0	0.70	0.84	0.18
1,2,4-triazole	**N1**	7	Ring deformation	901.6	0.72	0.85	0.53
		8	N-N stretch	923.9	1.27	1.13	
		10	C-N stretch	1107.5	0.50	0.71	
		13	C-N stretch	1286.2	0.39	0.62	
		14	C-N stretch	1540.8	0.32	0.57	
	N2	7	Ring deformation	1008.5	0.59	0.77	0.18
	N3	6	Ring deformation	961.5	0.84	0.92	0.10

smaller RMSDs for imine nitrogens when compared to amine nitrogens (as discussed in Sec. III B above).

D. Vibronic fine structures

Figures 1–3 present the simulated vibrationally resolved N 1*s* XPS spectra of all molecules, highlighting the distinct differences in binding energies of different core holes. Except for 2-pyrroline, all polynitrogen molecules exhibit well-separated spectral contributions from N1 and N2 (1,2,4-triazole shows well-separated contributions from N1, N2, and N3). Figures S2 to S13 display the atom-specific spectra of all molecules, revealing significant variations between the spectra of imine and amine nitrogens. The sum of FC factors for imine nitrogens rapidly converges at $n = 5$, whereas amine nitrogens require at least $n = 6$. The spectra of all imine nitrogens display two distinct characteristic peaks similar to pyridine (top of Fig. 1), primarily resulting from the 0-0 and 0-1 transitions (Figs. S2 to S13). In contrast, the spectra of amine nitrogens generally do not show a predominant 0-1 transition due to the significant mixing of various 0-*n* transitions. This often leads to multiple oscillationlike weak fingerprints within a broad peak, which exhibit less pronounced spectral features when observed at low resolution.

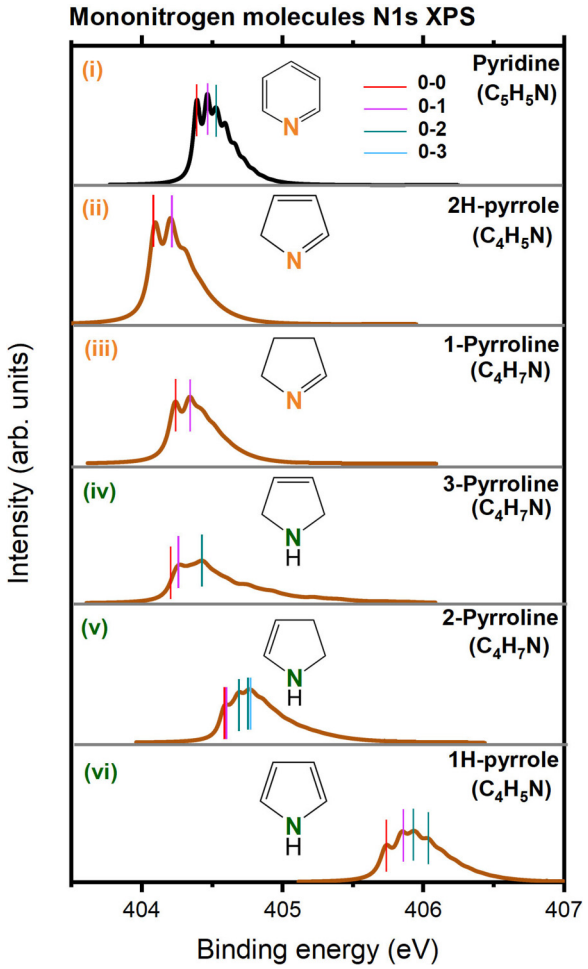

FIG. 1. Simulated vibrationally resolved N 1*s* XPS spectra of mononitrogen molecules (2H-pyrrole, 1-pyrroline, 3-pyrroline, 2-pyrroline, and 1H-pyrrole) using the FCH-DR method. Simulated pyridine spectrum from paper I [18] (black line, top) is also recaptured for comparison. In the structural illustrations, imine [green (i)–(iii)] and amine [orange (iv)–(vi)] nitrogens are distinguished. Sticks in different colors indicate different 0-*n* transitions (from left to right, with increasing *n*).

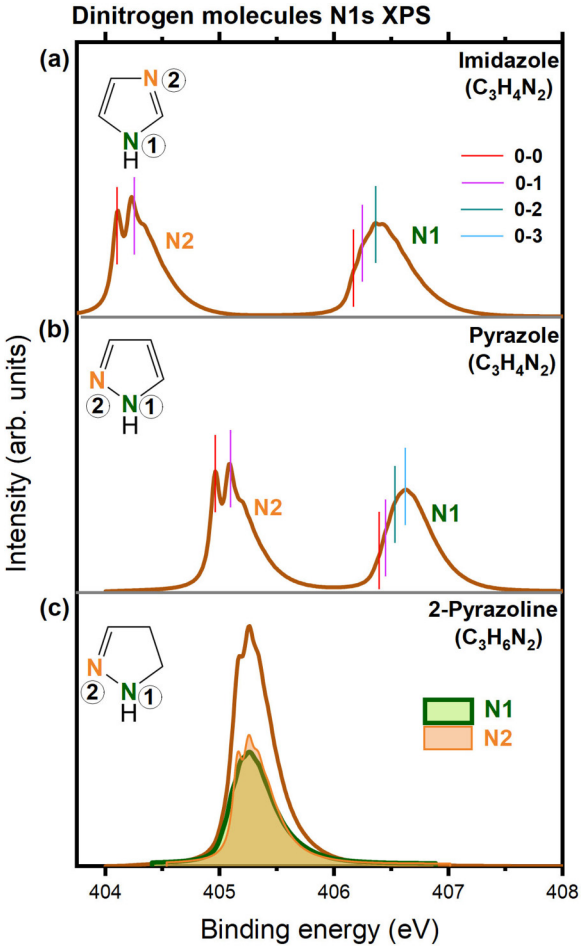

FIG. 2. Simulated vibrationally resolved N 1*s* XPS spectra of imidazole, pyrazole, and 2-pyrazoline. In panels (a) and (b), sticks in different colors indicate different 0-*n* transitions for each nitrogen (from left to right, with increasing *n*). In panel (c), the amine nitrogen N1 (green area, thick border) and the imine nitrogen N2 (orange area, thin border) contributions are indicated together with the total spectrum (brown thick line).

E. Effects of hydrogenation

Hydrogenation can lead to significant changes in vertical IPs, as shown in three pairs of examples in Fig. S14. Amine nitrogens experience a decrease in IPs of 1.2–1.4 eV, while imine nitrogens undergo an increase of approximately 0.2 eV in response to molecular hydrogenation.

Although hydrogenation has a significant effect on the IPs of amine and imine nitrogens, it has little impact on the spectral profile. For example, the vibrational characteristics of 1-pyrroline (Fig. S2) and 2H-pyrrole (Fig. S6), 2-pyrroline (Fig. S3) and 1H-pyrrole (Fig. S5), and N1/N2 of pyrazole (Fig. S8) and 2-pyrazoline (Fig. S9) are similar.

The hydrogenation does not affect the spectra of imine nitrogens but slows down the convergence of the spectra for amine nitrogens. For instance, the imine nitrogen spectra converge at $n = 5$ for both 1-pyrroline and 2H-pyrrole. N2 (imine) in pyrazole and 2-pyrazoline behave similarly. However, for amine nitrogen, 2-pyrroline ($n = 9$) is more difficult to converge than 1H-pyrrole ($n = 6$). Likewise, N1 (amine) of 2-pyrazoline and pyrazole converge at $n = 8$ and $n = 7$, respectively.

IV. DISCUSSION: GENERAL RULES FOR VIBRONIC COUPLING PROPERTIES IN SMALL *N*-HETEROCYCLES

In this section, we discuss general rules for vibronic coupling properties based on results of papers I [18], II [19], and III, covering mono- and bicyclic *N*-heterocycles. Special focus was paid to the difference between amine and imine nitrogens.

A. IPs

For all 35 *N*-heterocyclic molecules we have studied in this series, the vertical IPs lie within a range of 4.6 eV from 403.3 to 407.9 eV. The three families, namely five-membered rings (404.5–407.9 eV), six-membered rings (404.5–407.0 eV),

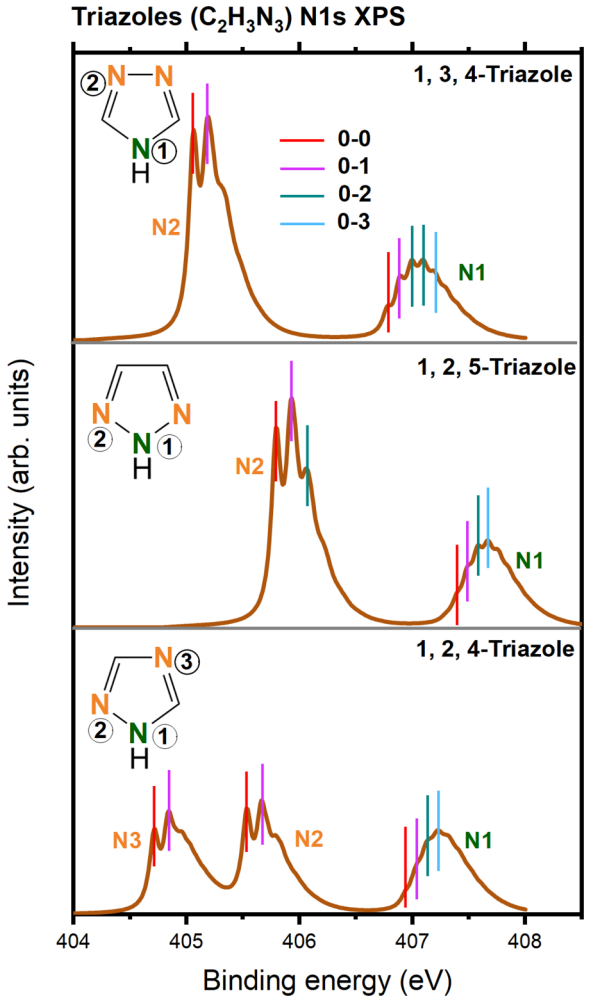

FIG. 3. Comparison of the simulated vibrationally resolved N 1*s* XPS spectra of 1,3,4-, 1,2,5-, and 1,2,4-triazoles. Sticks in different colors indicate different 0-*n* transitions of each nonequivalent nitrogen (from left to right, with increasing *n*; one exception is in the N1 spectrum of 1,3,4-triazole, where the two strongest peaks in green are both contributed by 0-2 transitions).

and bicyclic rings (403.3–407.2 eV), exhibit similar energy ranges. The connected N*-N bond tends to exhibit higher IPs for the N* core hole [18,19]. For example, the BEs of N1 (N2) exhibit relative chemical shifts of 0.2 eV (0.9 eV) for imidazole and pyrazole molecules with the meta- and orthopositions of the two nitrogens. The 1,3,4-triazole, 1,2,5-triazole, and 1,2,4-triazole molecules manifest the chemical environment around the N1 core hole as C-N*-C, N-N*-C, and N-N*-N, with corresponding vertical (adiabatic) ionization potentials of 407.2 (406.9), 407.4 (407.0), and 407.9 (407.4) eV, yielding relative chemical shifts of 0 (0), 0.2 (0.2), and 0.6 (0.5) eV, respectively. Obviously, these results are all due to the higher electronegativity of N atoms.

As depicted in Fig. 4, amine N atoms generally exhibit larger BEs than those of imine N atoms. With respect to ΔI, values associated with amine N atoms generally range between 0.3 and 0.5 eV, substantially larger than those of imine N atoms, which lie within the 0.1–0.2 eV range. Consequently, it can be inferred that the PES displacement pertaining to amine N atoms typically exceeds that of imine N atoms.

B. ZPE changes ($\Delta\varepsilon_0$)

Figure 5 shows the $\Delta\varepsilon_0$ values for each nonequivalent N in all 35 molecules. All 62 $\Delta\varepsilon_0$ values contributed from these nonequivalent nitrogen atoms cover a region of −0.10–0.05 eV, among which only six values are close to zero, indicating similar curvatures of PESs before and after the N 1*s* ionization. For those nonzero values, it is interesting to find that most, if not all, imine nitrogens give positive values, while amine nitrogens give negative values. This result indicates that the curvature generally becomes flatter (steeper) for amine (imine) N atoms. Nevertheless, exceptions indeed exist, particularly in six-membered *N*-heterocycles, where the positive and negative values are almost evenly distributed.

C. Vibrational reorganization energies

The 1*s* ionization on amine and imine nitrogens leads to distinctly different structural changes. The vibrational reorganization energies for each FCH state of all 35 molecules are listed in Tables III, S1, and S2, and are collectively visualized in Fig. 6. The ionization of amine nitrogens (0.3–0.9 eV) produces greater reorganization energies than imine nitrogens (0.1–0.3 eV). This indicates that amine nitrogens are more structurally altered than imine nitrogens during the N 1*s* ionization process.

D. Core ionization induced global and local structural changes

The conclusion above for E_r is consistent with the RMSD results between the ground state and the N 1*s* ionized state structures, where amine nitrogens (0.03–0.15 Å) generally exhibit larger RMSD values than imine nitrogens (0.03–0.05 Å).

Apart from the global geometrical changes, we also summarize the local changes at the ionization center (N*) for the series of molecules. The difference exists for nitrogens in five- and six-membered rings. For five-membered *N*-heterocycles, the bond length alternation (BLA) is consistent with the Kekulé structure, where the two N-*X* distances at each N site exhibit the distinct tendency of one longer and one shorter distance. In contrast, the BLA is more diminished for the six-membered ring structures, either in monocyclic [18] or bicyclic [19] molecules. That is because the difference between single and double bonds is effectively averaged within the conjugated π bond system and resonating Kekulé structures.

For the N*–*X* distances, amine N atoms (N_a^*–*X*, 1.40–1.56 Å) generally have a longer distance than imine N atoms (N_i^*-*X*, 1.25–1.50 Å). The N_a^*-*X* are always elongated, while N_i^*-*X* can be either elongated or shortened. The N_a^*-H bond lengths in amine nitrogens remain nearly constant at 0.97–0.98 Å and decrease only by 0.02–0.04 Å compared to the GS geometry.

As for the bond angles ∠C-N*-*X*, we found an increase for all imine N atoms (∠C-N_i^*-*X*). However, the bond angles ∠C-N_a^*-*X* for amine N atoms are decreased for most

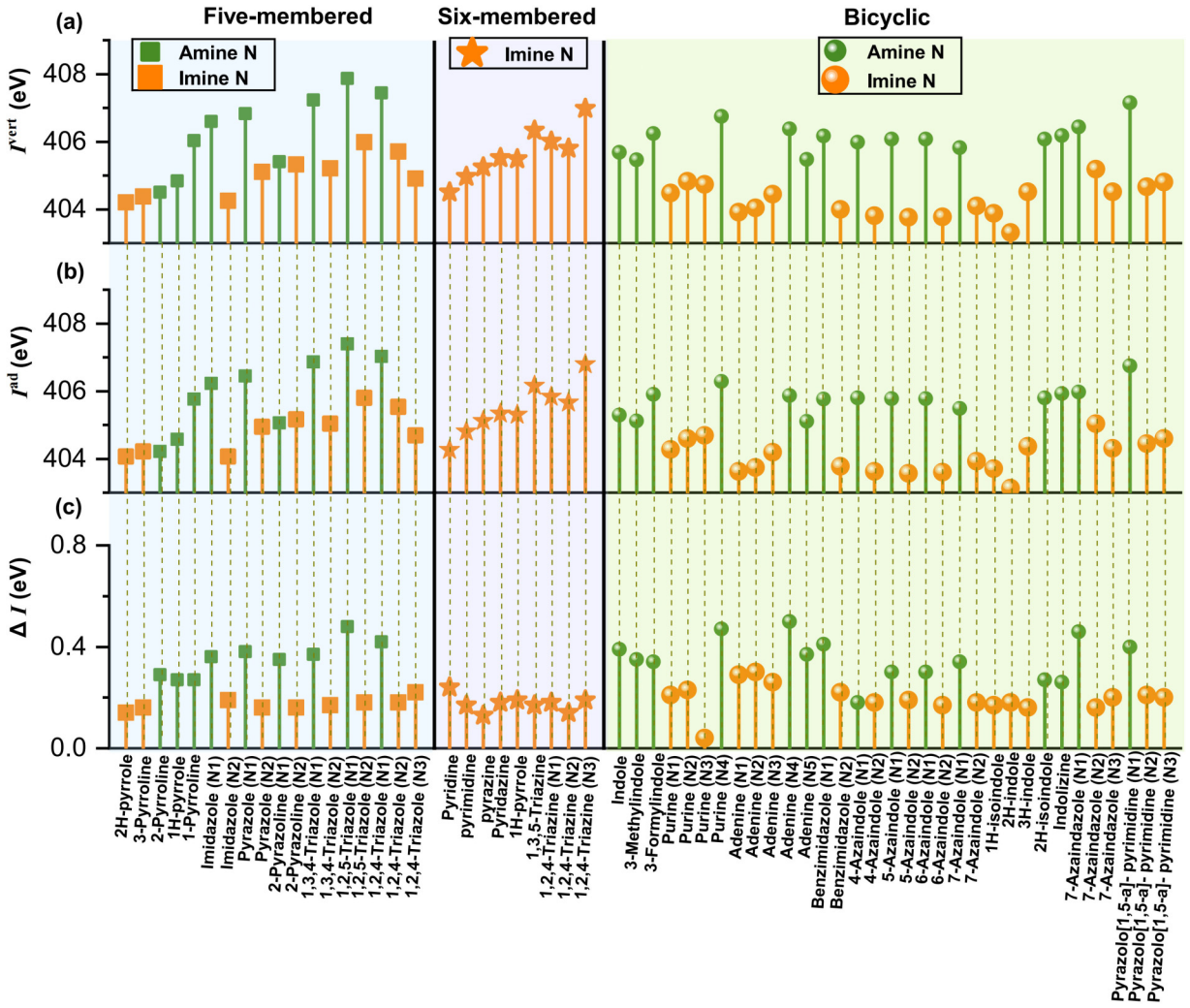

FIG. 4. Simulated (a) vertical (I^{vert}), (b) adiabatic (I^{ad}) ionization potentials, and (c) their difference (ΔI) of all 35 molecules studied in this series of papers [N-heterocycles with five-membered rings (this work), six-membered rings [18], and bicyclic rings [19]. Amine (green, small markers) and imine (orange, large markers) nitrogens are distinguished in color.

molecules, except for three nonplanar five-membered rings (2-pyrroline, 3-pyrroline, and N1 in 2-pyrazoline).

E. Active modes

The active ground-state vibrational modes of all 35 molecules are summarized in the Supplemental Material [69]. A threshold of HRF, $S_i \geqslant 0.3$, was adopted for all molecules. Within this standard, amine nitrogens usually exhibit more active vibrational modes (2–6 modes) compared to imine nitrogens (1–3 modes). For imine N 1*s* ionizations, we can consistently identify a ring deformation mode that involves mainly N* and the atom (C or N) in its paraposition. Concerning amine nitrogens, another type of ring deformation mode is commonly identified, which involves N* along with orthoposition atoms (C or N). No hydrogen vibrations (C-H stretching or bending) were found to be activated in the six-membered ring molecule. However, in both the five-membered and bicyclic molecules, active modes involving N/C-H bending are commonly found.

F. Characteristics and interpretations of vibronic fine structures

Generally, spectral profiles are related to the structural relaxation and vibrational coupling of the excited states [70]. An increase in structural alterations between the ground and excited states results in a broadening of the spectral width. As discussed above, an amine nitrogen usually exhibits larger RMSD and reorganization energy than an imine nitrogen, leading to a broader spectral profile contributed by the amine nitrogen. For vibrational modes that exhibit strong coupling with structural changes, the high-order vibrational transition could have significant contributions and lead to larger Stokes shifts to the spectra. Taking 1,3,4-triazole as an example, Fig. 7 analyzes the correlation between the structural changes induced by core ionization and the ground-state active mode. In Fig. 7(a), we observe that N1 (amine nitrogen) 1*s* ionization leads to a significant shortening of the adjacent C-N bond length (from 1.30 to 1.25 Å). This structural reorganization couples with modes 10 and 15, as depicted in Fig. 7(c), where mode 15 represents a strong electron-phonon coupling mode. Figure 7(b) shows that the prominent feature of the 1*s*

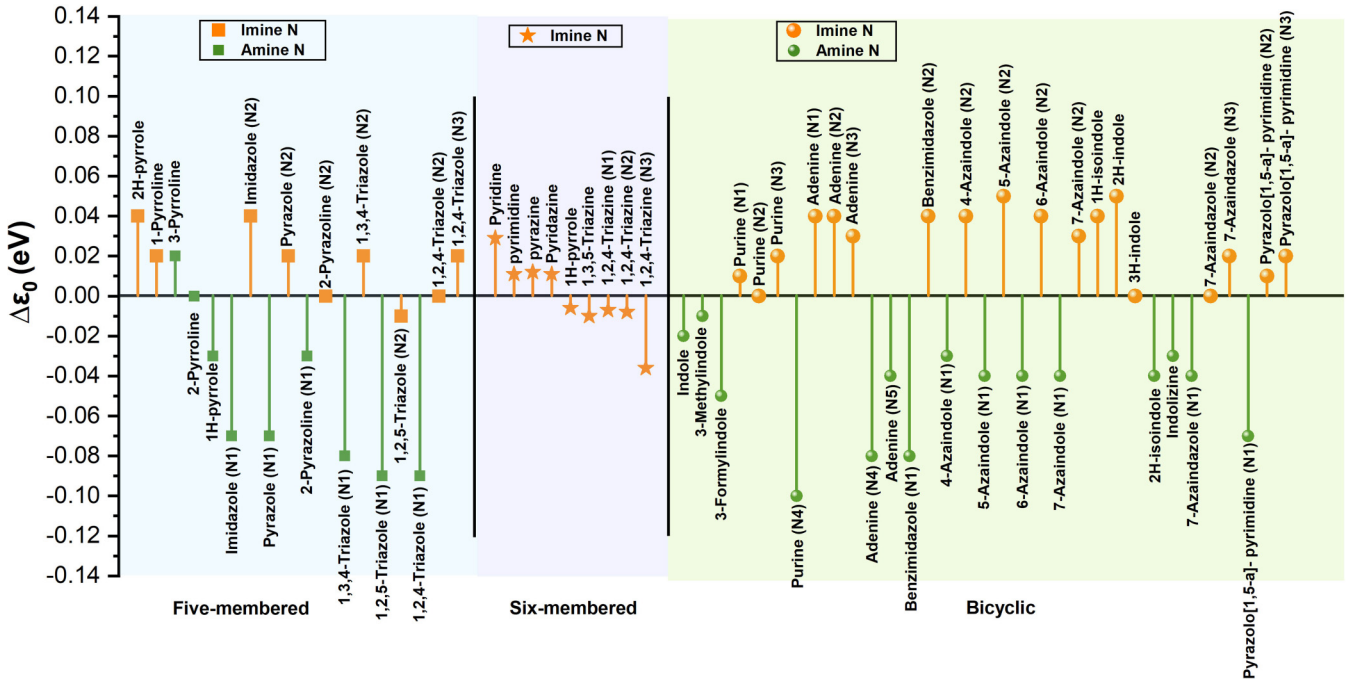

FIG. 5. Simulated $\Delta\varepsilon_0$ values of amine and imine nitrogens in all 35 molecules studied in this series of papers: *N*-heterocycles with five-membered rings (this work), six-membered rings [18], and bicyclic rings [19]. $\Delta\varepsilon_0$ of amine (green, small markers) and imine (orange, large markers) nitrogens are distinguished by colors.

ionization state of N2 (imine nitrogen) is the increase in the angle ∠C-N*-N (from 107.4 to 110.3°). Modes 6 and 9 couple with this structural change (corresponding HRFs are 0.56 and 0.30, respectively), but not as strongly as those observed for the case of N1. Consequently, the spectral signature of N2 (imine nitrogen) is dominated by the 0-1 transition, whereas the spectral profile of N1 (amine nitrogen) is dominated by the 0-*n* transition with a relatively large *n* ($n = 2$).

G. Effect of the benzene ring

To examine the effect of the benzene ring, i.e., five-membered monocyclic and bicyclic molecules, three pairs of molecules are compared (pyrrole and indole in Fig. 8, 1H-isoindole and 2H-pyrrole in Fig. S15, and imidazole and benzimidazole in Fig. 9). Within each pairing, the bicyclic molecules display a pronounced redshift in BEs relative to

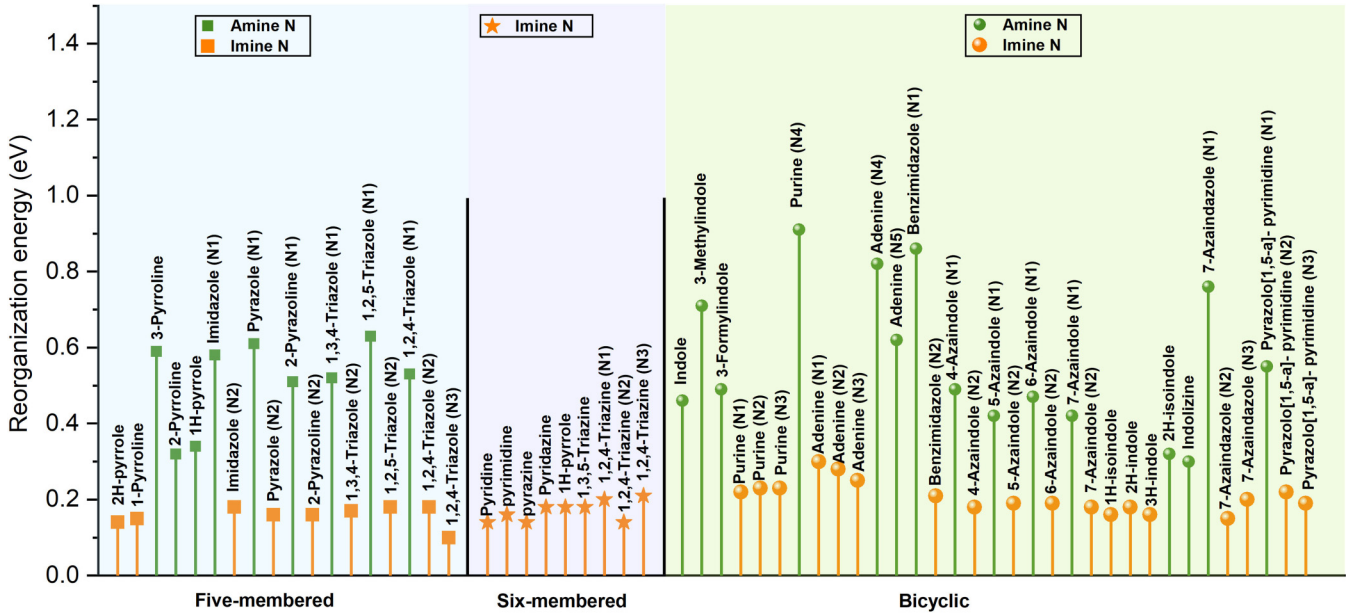

FIG. 6. Simulated reorganization energies for all 35 molecules studied in this series of papers: *N*-heterocycles with five-membered rings (this work), six-membered rings [18], and bicyclic rings [19]. Amine (green, small markers) and imine (orange, large markers) nitrogen atoms are distinguished by color.

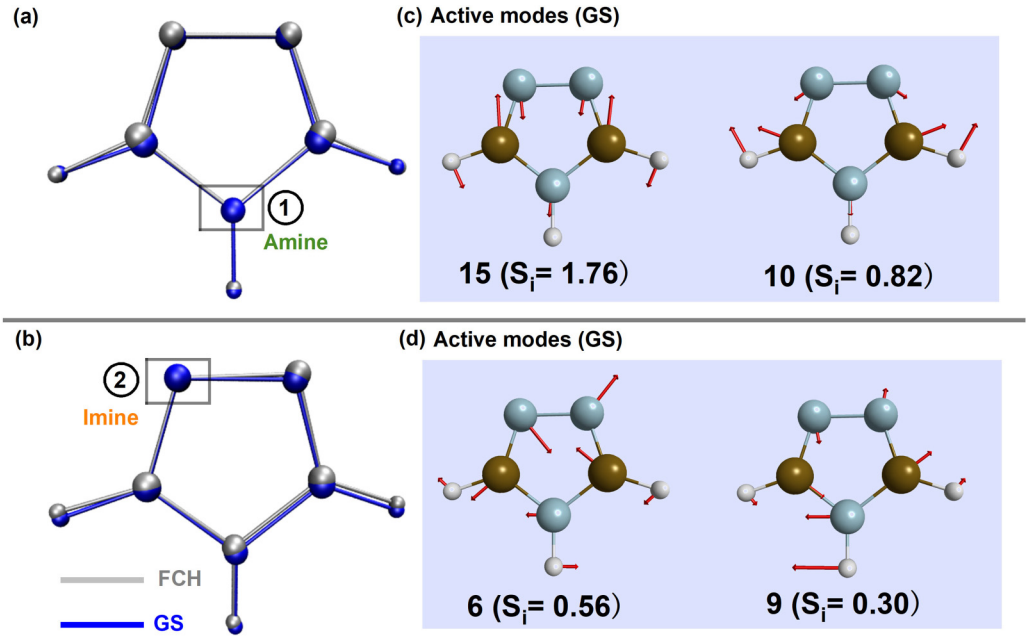

FIG. 7. Analyses for 1,3,4-triazole. (a),(b) Superposition of optimized geometries in the GS (blue, dark) and FCH (gray, light) states: (a) N1 (amine N) and (b) N2 (imine N) 1*s* ionizations. Core ionized center is indicated by a black square. (c),(d) GS active vibrational modes. The number indicates the mode index with the Huang-Rhys factor given in parentheses.

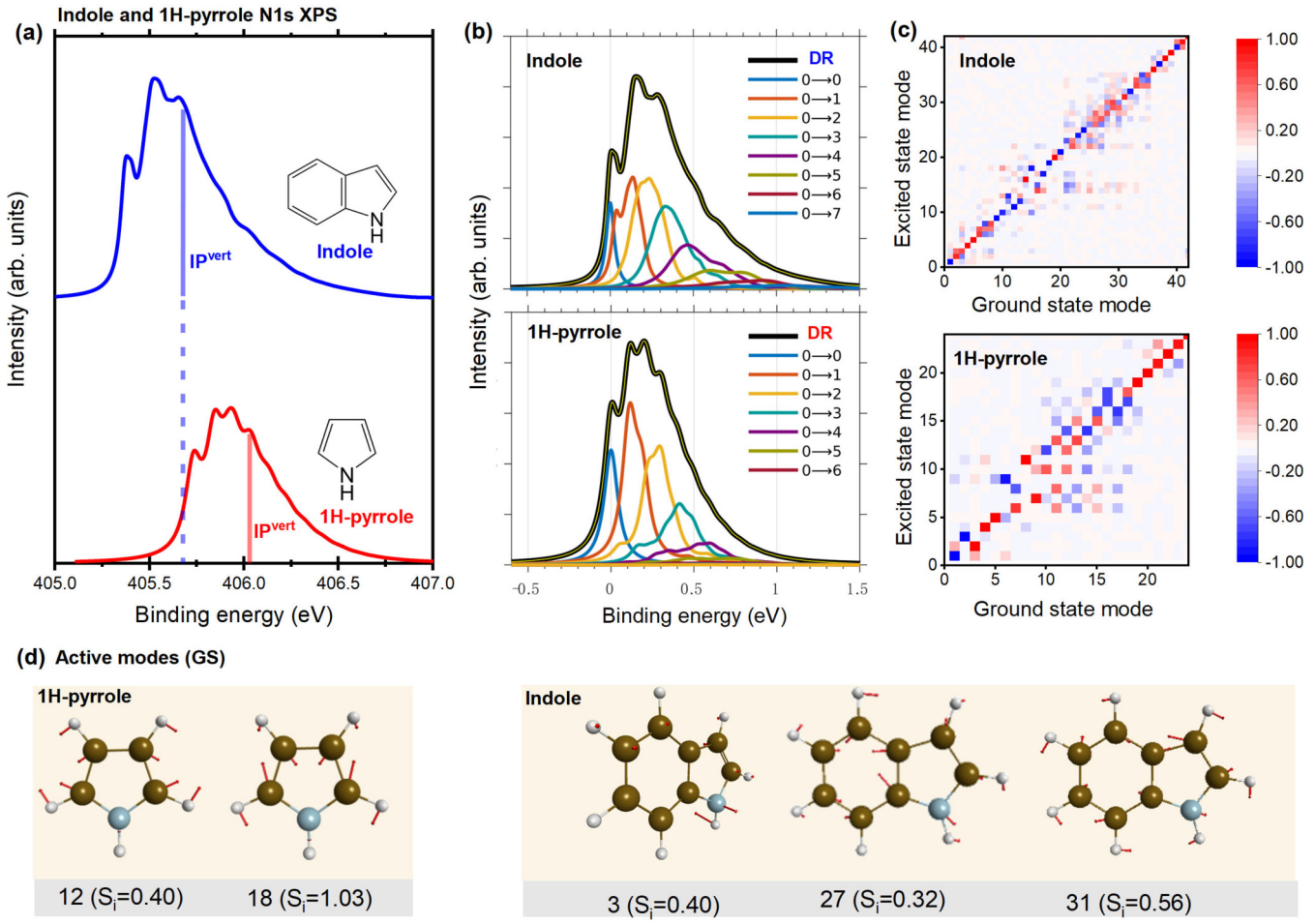

FIG. 8. Comparison of indole and 1H-pyrrole based on (a) spectra (vertical ionization energies are indicated by vertical lines), (b) contributions of various 0-*n* transitions to convergence, (c) elements of the Duschinsky matrix **J**, and (d) active modes.

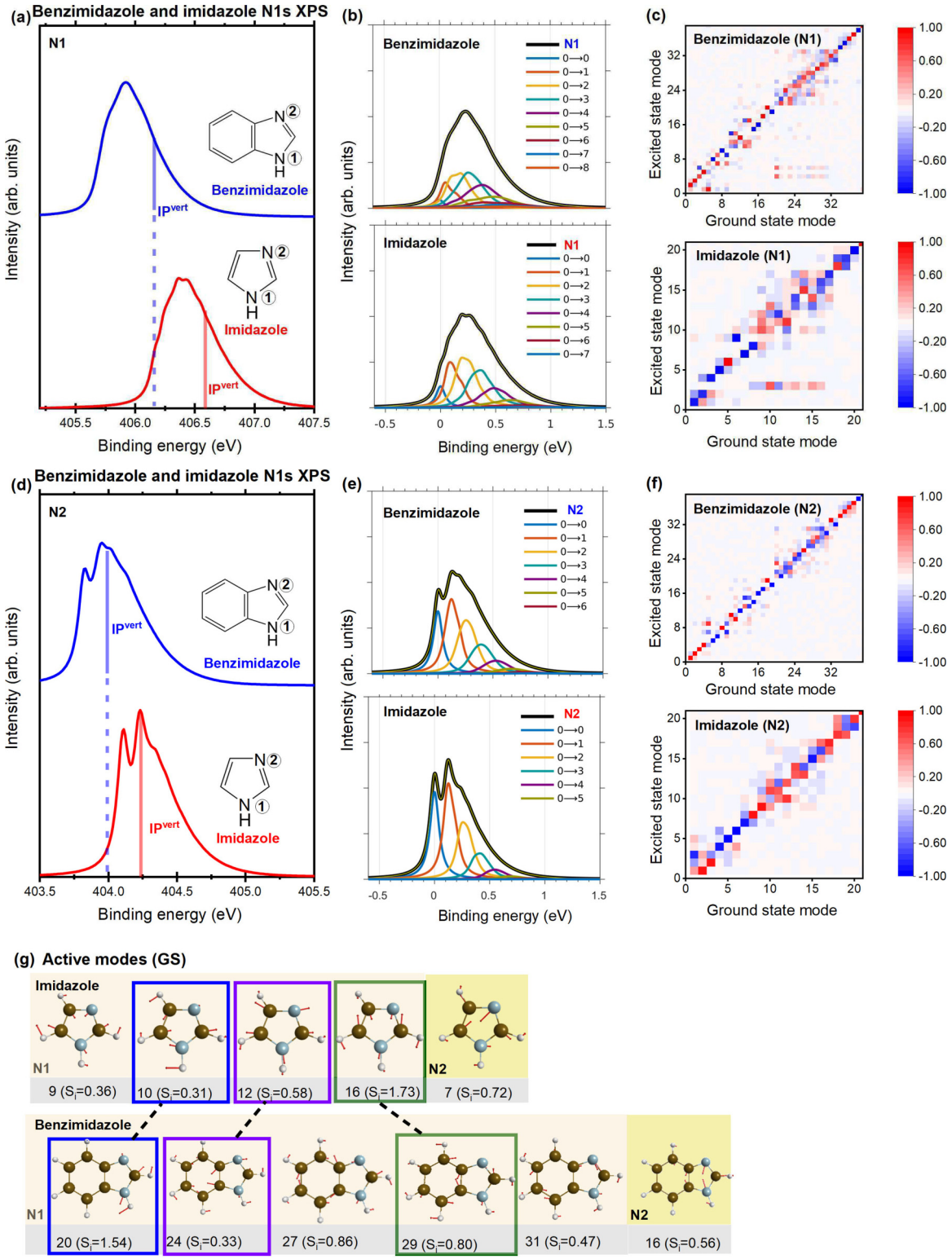

FIG. 9. Comparison of benzimidazole and imidazole based on (a), (d) spectra (vertical ionization energies are indicated by vertical lines), (b), (e) contributions of the various 0-*n* transitions to convergence (from left to right, with increasing *n*), (c), (f) elements of the Duschinsky matrix **J**, and (g) active modes. In panel (g), colored (blue, purple, and green) frames distinguish three types of modes, where in each type (connected by a dashed line), the vibration mode within the five-membered ring can be approximately tracked between the two molecules.

monocyclic molecules, attributable to the benzene ring acting as an electron-donating group (EDG). Regarding spectra, five-membered rings invariably converge at a faster rate than their bicyclic counterparts, consequently resulting in narrower profiles. This phenomenon can be attributed to the lesser total reorganization energy of five-membered ring molecules, as depicted in Table IV. We examined the Duschinsky matrix for each pair of molecules and found that the bicyclic molecules

TABLE IV. Total vibrational reorganization energy (E_r) and transition quantum number n (when the spectra achieve convergence) for three groups of monocyclic and bicyclic molecules.

Molecule	N*	E_r (eV)	n
1H-pyrrole	N	0.34	6
indole	N	0.46	7
2H-pyrrole	N	0.14	5
1H-isoindole	N	0.16	6
imidazole	N1	0.58	7
	N2	0.18	5
benzimidazole	N1	0.86	8
	N2	0.21	6

displayed a more pronounced mode mixing effect [Fig. 8(c), Figs. 9(c), 9(f) and Fig. S15(c)].

We have also conducted a comparison of the GS active modes for monocyclic and bicyclic molecules. As depicted in Figs. 8(d), 9(g), and S15(d), each selected molecule features one active vibrational mode for the imine nitrogens, while amine nitrogens in bicyclic molecules have more active modes. Although similar ring deformation modes are observed within the five-membered ring in both imidazole and benzimidazole, the vibrations of benzimidazole tend to be delocalized across both the five- and six-membered rings [Fig. 9(g)]. This result demonstrates that the introduction of a benzene ring can efficaciously alter the active modes.

V. CONCLUSIONS AND OUTLOOK

In summary, we have simulated the vibrationally resolved N 1*s* XPS spectra of 12 five-membered *N*-heterocyclic compounds using the B3LYP-DR method and carried out a comprehensive analysis on the N 1*s* binding energies, geometrical changes, major vibronic transitions, and active vibrational modes. A clear distinction between amine and imine nitrogens was found, which is consistent with previous studies (paper I [18] and paper II [19]).

Our series of investigations paint a comprehensive landscape for comprehending the N 1*s* vibronic fine structure in small *N*-heterocycles. For all 35 *N*-heterocycles in this series, the rules for vibronic coupling properties are summarized. Distinctive performance of amine and imine nitrogens are summarized as follows. (1) Energies. Amine nitrogens generally have larger 1*s* BEs than imine nitrogens and adjacent N-N bonds can increase the BEs. (2) Profiles. The spectra of imine nitrogens exhibit two distinct characteristic peaks originating from the 0-0 and 0-1 transitions, whereas the spectra of amine nitrogens are characterized by a broad peak with numerous weak fingerprints due to significant mixing of various 0-*n* transitions. (3) PES. N 1*s* ionization generally leads to a pronounced alteration in the curvature direction of the final-state PES, which became flatter (steeper) for amine (imine) N atoms. The PES displacement associated with amine N atoms generally surpasses that of imine N atoms. (4) Reorganization energy. Amine nitrogens always have greater total vibrational reorganization energy than imine nitrogens. (5) Structure. Ionization for amine N atoms instigates more substantial global structural alterations compared to imine N atoms, evidenced by the difference between vertical and adiabatic ionization energies, the RMSD between **min GS** and **min FCH**, and reorganization energy. (6) The 1*s* ionization in amine N atoms always elongates N*-C and shortens the N*-H bond lengths, while both elongation and shortening in N*-C bond lengths are observed for imine N atoms. Additionally, we also investigated the influence of benzene rings on vibronic coupling by comparing the properties of five-membered rings and bicyclic compounds.

ACKNOWLEDGMENTS

Financial support from the National Natural Science Foundation of China (Grant No. 12274229) is greatly acknowledged. M.W. thanks the Fund for Fostering Talented Doctoral Students of Nanjing University of Science and Technology.

[1] J. R. Rumble Jr., D. M. Bickham, and C. J. Powell, The nist x-ray photoelectron spectroscopy database, Surf. Interface Anal. **19**, 241 (1992).
[2] W. Jolly, K. Bomben, and C. Eyermann, Core-electron binding energies for gaseous atoms and molecules, At. Data Nucl. Data Tables **31**, 433 (1984).
[3] C. D. Wagner, *Handbook of X-ray Photoelectron Spectroscopy: A Reference Book of Standard Data for Use in X-ray Photoelectron Spectroscopy* (Perkin-Elmer, Shelton, CT, 1979).
[4] Https://www.xpsdata.com/, accessed on 2023-5-31.
[5] Https://www.xpslibrary.com/, accessed on 2023-5-31.
[6] Https://espectra.aip.org/, accessed on 2023-5-31.
[7] Http://www.sasj.jp/, accessed on 2023-5-31.
[8] Http://www.lasurface.com/xps/index, php accessed on 2023-5-31.
[9] K. Siegbahn, Electron spectroscopy for atoms, molecules, and condensed matter, Rev. Mod. Phys. **54**, 709 (1982).
[10] J. F. Watts and J. Wolstenholme, *An Introduction to Surface Analysis by XPS and AES* (Wiley-VCH, Weinheim, 2003), Chap. 5, p. 149.
[11] E. Sokolowski, C. Nordling, and K. Siegbahn, Magnetic analysis of x-ray produced photo and auger electrons, Ark. Fys. **12**, 301 (1957).
[12] K. Siegbahn, C. Nordling, A. Fahlman, R. Nordberg, K. Hamrin, J. Hedman, G. Johansson, T. Bergmark, S. Karlsson, I. Lindgren *et al.*, *ESCA: Atomic, Molecular and Solid State Structure Studies by Means of Electron Spectroscopy* (Almqvist & Wiksell, Uppsala, Sweden, 1967).
[13] K. Siegbahn, D. A. Allison, and J. H. Allison, *ESCA-Photoelectron Spectroscopy* (CRC Press, Cleveland, OH, 1974).
[14] D. Allison, G. Johansson, C. Allan, U. Gelius, H. Siegbahn, J. Allison, and K. Siegbahn, Molecular spectroscopy by means of ESCA, J. Electron Spectrosc. Relat. Phenom. **1**, 269 (1972).

[15] U. Gelius, P. F. Hedén, J. Hedman, B. J. Lindberg, R. Manne, R. Nordberg, C. Nordling, and K. Siegbahn, Molecular spectroscopy by means of ESCA III. *Carbon compounds*, Phys. Scr. **2**, 70 (1970).

[16] H. Fellner-Feldegg, H. Siegbahn, L. Asplund, P. Kelfve, and K. Siegbahn, ESCA applied to liquids IV. A wire system for ESCA measurements on liquids, J. Electron Spectrosc. Relat. Phenom. **7**, 421 (1975).

[17] H. Siegbarn, L. Asplund, P. Kelfve, K. Hamrin, L. Karlsson, and K. Siegbahn, ESCA applied to liquids. II. Valence and core electron spectra of formamide, J. Electron Spectrosc. Relat. Phenom. **5**, 1059 (1974).

[18] M. Wei, X. Cheng, L. Zhang, J.-R. Zhang, S.-Y. Wang, G. Ge, G. Tian, and W. Hua, Vibronic fine structure in the nitrogen 1s photoelectron spectra of molecules from Franck-Condon simulations: Azines, Phys. Rev. A **106**, 022811 (2022).

[19] M. Wei, L. Zhang, G. Tian, and W. Hua, Vibronic fine structure in the nitrogen 1 s photoelectron spectra from Franck-Condon simulation. II. Indoles, Phys. Rev. A **108**, 022816 (2023).

[20] M. Alongi, G. Minetto, and M. Taddei, New pyrrole-based amino acids for the synthesis of peptidomimetic constrained scaffolds, Tetrahedron Lett. **46**, 7069 (2005).

[21] N. R. Wurtz, J. M. Turner, E. E. Baird, and P. B. Dervan, Fmoc solid phase synthesis of polyamides containing pyrrole and imidazole amino acids, Org. Lett. **3**, 1201 (2001).

[22] M. J. Crossley and J. A. McDonald, Fused porphyrin-imidazole systems: new building blocks for synthesis of porphyrin arrays, J. Chem. Soc., Perkin Trans. **1**, 2429 (1999).

[23] C. Gomez, J.-F. Betzer, A. Voituriez, and A. Marinetti, Phosphine organocatalysis in the synthesis of natural products and bioactive compounds, ChemCatChem **5**, 1055 (2013).

[24] N. T. Nguyen, V. V. Dai, A. Mechler, N. T. Hoa, and Q. V. Vo, Synthesis and evaluation of the antioxidant activity of 3-pyrroline-2-ones: experimental and theoretical insights, RSC Adv. **12**, 24579 (2022).

[25] G. Sun, X. Zou, J. Wang, and W. Yang, Sulfur-directed palladium-catalyzed C(sp^3)–H α-arylation of 3-pyrrolines: easy access to diverse polysubstituted pyrrolidines, Org. Chem. Front. **7**, 666 (2020).

[26] W. K. Anderson and A. S. Milowsky, 3-Pyrroline N-oxide bis(carbamate) tumor inhibitors as analogs of indicine N-oxide, J. Med. Chem. **30**, 2144 (1987).

[27] M. Chen, L. Zhang, A. Lu, X. Wang, W. Si, J. Yan, and C. Yang, Novel carboxylated pyrroline-2-one derivatives bearing a phenylhydrazine moiety: Design, synthesis, antifungal evaluation and 3D-QSAR analysis, Bioorg. Med. Chem. Lett. **30**, 127519 (2020).

[28] A. Kost and I. Grandberg, Progress in pyrazole chemistry, *Advances in Heterocyclic Chemistry* (Elsevier, Amsterdam, 1966), Vol. 6, pp. 347–429.

[29] A. A. Dippold and T. M. Klapötke, A Study of dinitro-bis-1,2,4-triazole-1,1'-diol and derivatives: Design of high-performance insensitive energetic materials by the introduction of N-oxides, J. Am. Chem. Soc. **135**, 9931 (2013).

[30] J. Ma, G. Cheng, X. Ju, Z. Yi, S. Zhu, Z. Zhang, and H. Yang, Amino-nitramino functionalized triazolotriazines: a good balance between high energy and low sensitivity, Dalton Trans. **47**, 14483 (2018).

[31] P. Wang, Y. Xu, Q. Lin, and M. Lu, Recent advances in the syntheses and properties of polynitrogen pentazolate anion *cyclo*-N_5^- and its derivatives, Chem. Soc. Rev. **47**, 7522 (2018).

[32] C. Zhang, C. Sun, B. Hu, C. Yu, and M. Lu, Synthesis and characterization of the pentazolate anion *cyclo*-N_5^- in $(N_5)_6(H_3O)_3(NH_4)_4$ Cl, Science **355**, 374 (2017).

[33] Y. Yao, Q. Lin, X. Zhou, and M. Lu, Recent research on the synthesis pentazolate anion *cyclo*-N_5^-, FirePhysChem **1**, 33 (2021).

[34] U. Gelius, C. J. Allan, G. Johansson, H. Siegbahn, D. A. Allison, and K. Siegbahn, The ESCA spectra of benzene and the Iso-electronic series, thiophene, pyrrole and furan, Phys. Scr. **3**, 237 (1971).

[35] F.-M. Pan, P. C. Stair, and T. H. Fleisch, Chemisorption of pyridine and pyrrole on iron oxide surfaces studied by XPS, Surf. Sci. **177**, 1 (1986).

[36] R. G. Cavell and D. A. Allison, Site of protonation in aromatic and acyclic amines and acyclic amides revealed by N1s core level electron spectroscopy, J. Am. Chem. Soc. **99**, 4203 (1977).

[37] D. Nolting, N. Ottosson, M. Faubel, I. V. Hertel, and B. Winter, Pseudoequivalent nitrogen atoms in aqueous imidazole distinguished by chemical shifts in photoelectron spectroscopy, J. Am. Chem. Soc. **130**, 8150 (2008).

[38] D. Clark and D. Lilley, Molecular core binding energies for some five membered ring heterocycles as determined by X-ray photoelectron spectroscopy, Chem. Phys. Lett. **9**, 234 (1971).

[39] X. Du, S.-Y. Wang, M. Wei, J.-R. Zhang, G. Ge, and W. Hua, A theoretical library of N1s core binding energies of polynitrogen molecules and ions in the gas phase, Phys. Chem. Chem. Phys. **24**, 8196 (2022).

[40] W. Hua, B. Gao, S. Li, H. Ågren, and Y. Luo, Refinement of DNA structures through near-edge x-ray absorption fine structure analysis: Applications on guanine and cytosine nucleobases, nucleosides, and nucleotides, J. Phys. Chem. B **114**, 13214 (2010).

[41] S. C. Cosgrove, A. Brzezniak, S. P. France, J. I. Ramsden, J. Mangas-Sanchez, S. L. Montgomery, R. S. Heath, and N. J. Turner, Imine reductases, reductive aminases, and amine oxidases for the synthesis of chiral amines: Discovery, characterization, and synthetic applications, *Methods in Enzymology* (Elsevier, Amsterdam, 2018), Vol. 608, pp. 131–149.

[42] T. P. Mohammed, A. George, M. P. Sivaramakrishnan, P. Vadivelu, S. Balasubramanian, and M. Sankaralingam, Deciphering the effect of amine versus imine ligands of copper(II) complexes in 2-aminophenol oxidation, J. Inorg. Biochem. **247**, 112309 (2023).

[43] H. Vardhan, A. Mehta, I. Nath, and F. Verpoort, Dynamic imine chemistry in metal–organic polyhedra, RSC Adv. **5**, 67011 (2015).

[44] H. Chen, H. Ye, Y. Hai, L. Zhang, and L. You, n $\rightarrow \pi^*$ interactions as a versatile tool for controlling dynamic imine chemistry in both organic and aqueous media, Chem. Sci. **11**, 2707 (2020).

[45] C. Qian, L. Feng, W. L. Teo, J. Liu, W. Zhou, D. Wang, and Y. Zhao, Imine and imine-derived linkages in two-dimensional covalent organic frameworks, Nat. Rev. Chem. **6**, 881 (2022).

[46] H. Liu, J. Chu, Z. Yin, X. Cai, L. Zhuang, and H. Deng, Covalent organic frameworks linked by amine bonding for concerted electrochemical reduction of CO_2, Chem **4**, 1696 (2018).

[47] M. W. Schmidt, K. K. Baldridge, J. A. Boatz, S. T. Elbert, M. S. Gordon, J. H. Jensen, S. Koseki, N. Matsunaga, K. A. Nguyen, S. Su, T. L. Windus, M. Dupuis, and J. A. Montgomery, General

atomic and molecular electronic structure system, J. Comput. Chem. **14**, 1347 (1993).

[48] M. S. Gordon and M. W. Schmidt, Advances in electronic structure theory: GAMESS a decade later, *Theory and Applications of Computational Chemistry* (Elsevier, Amsterdam, 2005), pp. 1167–1189.

[49] A. D. Becke, Density-functional exchange-energy approximation with correct asymptotic behavior, Phys. Rev. A **38**, 3098 (1988).

[50] A. D. Becke, A new mixing of Hartree–Fock and local density-functional theories, J. Chem. Phys. **98**, 1372 (1993).

[51] C. Lee, W. Yang, and R. G. Parr, Development of the Colle-Salvetti correlation-energy formula into a functional of the electron density, Phys. Rev. B **37**, 785 (1988).

[52] G. Tian, S. Duan, W. Hua, and Y. Luo, DynaVib, version 1.0, Royal Institute of Technology, Sweden, 2012.

[53] W. Hua, G. Tian, and Y. Luo, Theoretical assessment of vibrationally resolved C1s X-ray photoelectron spectra of simple cyclic molecules, Phys. Chem. Chem. Phys. **22**, 20014 (2020).

[54] F. Duschinsky, The importance of the electron spectrum in multi atomic molecules. Concerning the Franck-Condon principle, Acta Physicochim. URSS **7**, 551 (1937).

[55] T. Sharp and H. Rosenstock, Franck-Condon factors for polyatomic molecules, J. Chem. Phys. **41**, 3453 (1964).

[56] P. T. Ruhoff, Recursion relations for multi-dimensional Franck-Condon overlap integrals, Chem. Phys. **186**, 355 (1994).

[57] P. T. Ruhoff and M. A. Ratner, Algorithms for computing Franck-Condon overlap integrals, Int. J. Quantum Chem. **77**, 383 (2000).

[58] O. Plashkevych, T. Privalov, H. Ågren, V. Carravetta, and K. Ruud, On the validity of the equivalent cores approximation for computing X-ray photoemission and photoabsorption spectral bands, Chem. Phys. **260**, 11 (2000).

[59] P. Macak, Y. Luo, and H. Ågren, Simulations of vibronic profiles in two-photon absorption, Chem. Phys. Lett. **330**, 447 (2000).

[60] L. Triguero, O. Plashkevych, L. Pettersson, and H. Ågren, Separate state vs. transition state Kohn-Sham calculations of X-ray photoelectron binding energies and chemical shifts, J. Electron Spectrosc. Relat. Phenom. **104**, 195 (1999).

[61] C. Nicolas and C. Miron, Lifetime broadening of core-excited and -ionized states, J. Electron Spectrosc. Relat. Phenom. **185**, 267 (2012).

[62] R. C. Couto, W. Hua, R. Lindblad, L. Kjellsson, S. L. Sorensen, M. Kubin, C. Bülow, M. Timm, V. Zamudio-Bayer, B. Von Issendorff, J. Söderström, J. T. Lau, J.-E. Rubensson, H. Ågren, and V. Carravetta, Breaking inversion symmetry by protonation: experimental and theoretical NEXAFS study of the diazynium ion, N_2 H^+, Phys. Chem. Chem. Phys. **23**, 17166 (2021).

[63] Http://jszy.njust.edu.cn/lxy/hwj_en/list.psp, accessed on 2024-2-18.

[64] P. S. Bagus, C. Sousa, and F. Illas, Consequences of electron correlation for XPS binding energies: Representative case for C(1s) and O(1s) XPS of CO, J. Chem. Phys. **145**, 144303 (2016).

[65] N. P. Bellafont, F. Illas, and P. S. Bagus, Validation of Koopmans' theorem for density functional theory binding energies, Phys. Chem. Chem. Phys. **17**, 4015 (2015).

[66] N. P. Bellafont, P. S. Bagus, and F. Illas, Prediction of core level binding energies in density functional theory: Rigorous definition of initial and final state contributions and implications on the physical meaning of Kohn-Sham energies, J. Chem. Phys. **142**, 214102 (2015).

[67] N. Pueyo Bellafont, F. Viñes, and F. Illas, Performance of the TPSS functional on predicting core level binding energies of main group elements containing molecules: A good choice for molecules adsorbed on metal surfaces, J. Chem. Theory Comput. **12**, 324 (2016).

[68] S. Atahan-Evrenk, A quantitative structure–property study of reorganization energy for known p-type organic semiconductors, RSC Adv. **8**, 40330 (2018).

[69] See Supplemental Material at http://link.aps.org/supplemental/10.1103/PhysRevA.109.022820 for visualization of amine and imine IPs, theoretical spectra of 12 individual five-membered *N*-heterocycles with analysis, additional examples for effects of hydrogenation and benzene rings, additional vibrational analyses, and energies of all 35 *N*-heterocycles.

[70] X. Qiu, G. Tian, C. Lin, Y. Pan, X. Ye, B. Wang, D. Ma, D. Hu, Y. Luo, and Y. Ma, Narrowband emission from organic fluorescent emitters with dominant low-frequency vibronic coupling, Adv. Opt. Mater. **9**, 2001845 (2021).